SCIENCE CHINA
Information Sciences

• RESEARCH PAPER •

April 2026, Vol. 69, Iss. 4, 140204:1–140204:18
https://doi.org/10.1007/s11432-025-4825-9

Special Topic: Logical System Control

A dimension-keeping semi-tensor product framework for compressed sensing

Qi QI[1], Abdelhamid TAYEBI[2,3], Daizhan CHENG[4] & Jun-E FENG[2*]

[1]*Mathematical Research Center, Shandong University, Jinan 250100, China*
[2]*School of Mathematics, Shandong University, Jinan 250100, China*
[3]*Department of Electrical Engineering, Lakehead University, Thunder Bay P7B 5E1, Canada*
[4]*Key Laboratory of Systems and Control, Chinese Academy of Sciences, Beijing 100190, China*

Received 8 September 2025/Revised 11 November 2025/Accepted 29 December 2025/Published online 11 March 2026

Abstract In compressed sensing (CS), sparse signals can be reconstructed from significantly fewer samples than required by the Nyquist-Shannon sampling theorem. While non-sparse signals can be sparsely represented in appropriate transformation domains, conventional CS frameworks rely on the incoherence of the measurement matrix columns to guarantee reconstruction performance. This paper proposes a novel method termed dimension-keeping semi-tensor product compressed sensing (DK-STP-CS), which leverages intra-group correlations while maintaining inter-group incoherence to enhance the measurement matrix design. Specifically, the DK-STP algorithm is integrated into the design of the sensing matrix, enabling dimensionality reduction while preserving signal recovery capability. For image compression and reconstruction tasks, the proposed method achieves notable noise suppression and improves visual fidelity. Experimental results demonstrate that DK-STP-CS significantly outperforms traditional CS and STP-CS approaches, as evidenced by higher peak signal-to-noise ratio (PSNR) values between the reconstructed and original images. The robustness of DK-STP-CS is further validated under noisy conditions and varying sampling rates, highlighting its potential for practical applications in resource-constrained environments.

Keywords compressed sensing, semi-tensor product, dimension-keeping semi-tensor product, image reconstruction, noise reduction

Citation Qi Q, Tayebi A, Cheng D Z, et al. A dimension-keeping semi-tensor product framework for compressed sensing. Sci China Inf Sci, 2026, 69(4): 140204, https://doi.org/10.1007/s11432-025-4825-9

1 Introduction

1.1 Background

Compressed sensing (CS), a revolutionary paradigm in signal processing, has emerged as a powerful methodology for reconstructing sparse signals from sub-Nyquist measurements [1,2]. The fundamental premise of CS lies in exploiting signal sparsity, where a vector $\mathbf{x}$ is considered k-sparse ($\mathbf{x} \in \Sigma_k$) if it contains at most k non-zero elements.

Traditional signal acquisition frameworks, governed by the Nyquist sampling theorem [3], require uniform sampling at twice the highest signal frequency. However, the exponential growth of data in modern digital systems renders Nyquist-rate sampling increasingly impractical due to excessive storage and computational demands. This limitation has motivated the development of CS, which fundamentally differs from conventional approaches through two key innovations: (1) non-uniform sampling strategies that maintain measurement incoherence, and (2) sparse signal recovery from significantly fewer measurements than required by the Nyquist criteria. While CS initially assumes signal sparsity, practical implementations extend this framework to non-sparse signals through sparse representation in appropriate transformation domains [4]. This generalization enables efficient compression of diverse real-world signals while preserving essential information.

The standard framework of CS is a special case of underdetermined linear equations

$$\mathbf{y} = \mathbf{A}\mathbf{x}, \tag{1}$$

where $\mathbf{A} \in \mathcal{M}_{m\times n}, \mathbf{x} \in \mathbb{R}^n, \mathbf{y} \in \mathbb{R}^m, m \ll n$. Vector $\mathbf{x}$ is the input signal and vector $\mathbf{y}$ is the compressed signal. Vector $\mathbf{x}$ cannot be obtained directly from the above equation, but if $\mathbf{x}$ is sparse in some transformation domain, one can obtain an approximate solution for $\mathbf{x}$. In fact, vector $\mathbf{x}$ can be expressed as

$$\mathbf{x} = \Theta\mathbf{s}, \tag{2}$$

* Corresponding author (email: fengjune@sdu.edu.cn)

where Θ is a sparsifying dictionary and $\mathbf{s}$ is a sparse vector. Thus,

$$\mathbf{y} = \mathbf{A}\Theta\mathbf{s} = \mathbf{\Psi}\mathbf{s}. \tag{3}$$

In the conventional CS paradigm, measurement matrices are inherently non-adaptive, implying that the rows of the sensing matrix $\mathbf{\Psi}$ are predefined and remain invariant throughout the acquisition process, independent of any prior measurement outcomes. However, adaptive sensing strategies, where subsequent measurement matrices are dynamically adjusted based on previously observed data, have been shown in specific scenarios to achieve substantial improvements in reconstruction accuracy or sampling efficiency. Theoretical and practical studies highlight that such adaptability can yield enhanced performance bounds, particularly in resource-constrained or noise-dominated environments. A solution to the underdetermined linear equation (3) can be found through the following optimization:

$$\min_{\mathbf{s}} \|\mathbf{s}\|_0 \quad \text{subject to} \quad \mathbf{y} = \mathbf{\Psi}\mathbf{s}, \tag{4}$$

where $\|\mathbf{s}\|_0$ denotes the l_0 norm of the vector $\mathbf{s}$. It represents the number of non-zero elements in the vector $\mathbf{s}$. In fact, one can show that for a general matrix $\mathbf{\Psi}$, even finding a solution that approximates the true minimum is NP-hard [5]. Since Eq. (4) is difficult to solve, problem (4) can be transformed, for an approximate solution, into the following problem [6,7]:

$$\min_{\mathbf{s}} \|\mathbf{s}\|_1 \quad \text{subject to} \quad \mathbf{y} = \mathbf{\Psi}\mathbf{s}, \tag{5}$$

where $\|\mathbf{s}\|_1$ denotes the l_1 norm of the vector $\mathbf{s}$. The design of the sensing matrix $\mathbf{\Psi}$ satisfying the restricted isometry property (RIP) [5,8] is an important problem. The measurement matrix $\mathbf{A}$ satisfies the RIP of order k if there exists a $\delta_k^{\mathbf{A}} \in (0,1)$ such that

$$(1-\delta_k^{\mathbf{A}})\|\mathbf{x}\|_2^2 \leqslant \|\mathbf{A}\mathbf{x}\|_2^2 \leqslant (1+\delta_k^{\mathbf{A}})\|\mathbf{x}\|_2^2. \tag{6}$$

The use of random matrices to construct the measurement matrix $\mathbf{A}$ offers several advantages, particularly in the context of the RIP. First, random measurement systems exhibit some robust characteristics, allowing the feasibility of the signal recovery even when a subset of measurements is corrupted or lost, provided the retained subset is sufficiently large [9]. This property ensures inherent robustness to measurement errors in compressive sensing frameworks. Second, in practical scenarios where a signal x is sparse under a specific transform basis Θ, the critical requirement shifts to ensuring that the matrix product $\mathbf{A}\Theta$ satisfies the RIP. Unlike deterministic constructions, which necessitate explicit structural alignment between $\mathbf{A}$ and Θ, random matrix designs are more general. For instance, if $\mathbf{A}$ is drawn from a Gaussian distribution and Θ is an orthonormal basis, the product $\mathbf{A}\Theta$ retains Gaussian properties, thereby satisfying the RIP with high probability. Notably, this universality extends beyond Gaussian distributions—rigorous theoretical analyses confirm analogous results for sub-Gaussian distributions and broader classes of random matrices. This universality principle underscores a key advantage of random constructions, enabling robust performance across diverse sparse representation bases without requiring prior knowledge of Θ.

CS has revolutionized signal acquisition and reconstruction by enabling the recovery of sparse signals from measurements, thereby alleviating the stringent requirements imposed by traditional sampling paradigms. Despite its theoretical elegance and broad applicability, conventional CS frameworks face practical challenges in resource-constrained environments, particularly concerning the storage and transmission of large measurement matrices. These matrices, often randomly constructed, must satisfy strict incoherence and RIP to guarantee reconstruction fidelity, yet their size grows substantially with signal dimension, leading to increased memory and bandwidth costs. But there is no doubt that compressive sensing has had a significant impact in many fields, such as medical imaging, wireless sensor networks, and real-time video processing, where both accuracy and efficiency are paramount.

1.2 Related work and motivation

The foundation of CS was established by the seminal studies of Donoho [1] and Candès et al. [5], which demonstrated that sparse or compressible signals can be accurately reconstructed from far fewer samples than required by the Nyquist-Shannon theorem. This breakthrough has led to widespread applications in medical [10] and SAR imaging [11], computational photography [12], and radar [13] and sensor networks [14]. The core of CS lies in solving an underdetermined linear system $\mathbf{y} = \mathbf{\Psi}\mathbf{s}$, where $\mathbf{\Psi} = \mathbf{A}\Theta$ is the sensing matrix, through sparsity-promoting optimization such as ℓ_1-minimization [6,7]. A critical factor in CS performance is the design of the measurement matrix $\mathbf{A}$. Early approaches favored random matrices (e.g., Gaussian, Bernoulli) due to their probabilistic satisfaction of the RIP [8] and universal incoherence [9]. However, such matrices are unstructured and require significant storage and transmission overhead, limiting their practicality in resource-constrained systems. To address these limitations, structured matrix designs have been explored. For instance, Toeplitz [15] and circulant matrices reduce storage

requirements by leveraging shift-invariant structures. Chaotic sensing operators [16] have also been proposed for their deterministic yet incoherent properties. While these methods improve efficiency, they often trade off flexibility and reconstruction quality, especially under low sampling rates or noisy conditions.

More recently, the semi-tensor product (STP) [17] has been introduced as a generalized matrix multiplication that operates across dimension-mismatched matrices. STP-based CS (STP-CS) [18] reduces the size of the measurement matrix by employing a Kronecker product structure $\mathbf{A} \otimes \mathbf{I}_\gamma$, thus lowering storage and transmission costs. However, STP-CS still relies on identity-based expansion, which does not fully exploit intra-signal correlations and may lead to suboptimal reconstruction under noise. Another line of research focuses on adaptive sensing and learning-based matrix designs [19]. Deep learning has emerged as a pivotal tool in CS. As reviewed in [20], the evolution of CS methodologies has been significantly influenced by learning-based approaches. For instance, Ref. [21] introduced a CNN-based reconstruction network that substantially reduces computational complexity. Further advancing this direction, Ref. [22] proposed an interpretable deep network inspired by the iterative shrinkage-thresholding algorithm (ISTA), which enhances both reconstruction accuracy and visual quality. Meanwhile, Ref. [23] presented a comprehensive deep learning framework that mitigates the common issue of blocking artifacts in recovered images. Collectively, these studies illustrate how deep learning has been integrated into the CS pipeline, facilitating the transition from traditional iterative methods to efficient non-iterative reconstruction algorithms.

The primary motivation for developing DK-STP-CS stems from three critical limitations in existing compressed sensing frameworks: (1) conventional CS requires storing and transmitting large measurement matrices, creating substantial resource overhead; (2) STP-CS, while reducing matrix size, fails to fully exploit the inherent correlations within signal groups; and (3) both approaches demonstrate limited robustness under noisy conditions and low sampling rates. Our DK-STP-CS framework is specifically designed to address these limitations by introducing a novel dimension-keeping semi-tensor product operation that simultaneously achieves measurement matrix compression, enhanced correlation exploitation, and improved noise robustness.

1.3 Contributions

This paper introduces a novel framework termed dimension-keeping semi-tensor product compressed sensing (DK-STP-CS), which leverages a generalized matrix operation to reduce the size of the measurement matrix while preserving and even enhancing reconstruction quality. By incorporating intra-group correlations and maintaining inter-group incoherence, DK-STP-CS achieves a more efficient use of structural information within the signal, leading to improved noise robustness and higher visual fidelity in image reconstruction tasks.

The main contributions of this work are as follows.

- We propose a novel compressed sensing framework, termed DK-STP-CS, which integrates the weighted dimension-keeping semi-tensor product (DK-STP) operation into the sensing matrix design.
- Our approach reduces the resource overhead associated with large measurement matrices in CS, making the method more suitable for memory and bandwidth limited applications.
- Our proposed approach improves the reconstruction quality under practical conditions, including noise and variable sampling rates, by exploiting structural properties of signals through a novel algebraic framework.
- Extensive comparative experiments are provided to illustrate the effectiveness of the proposed approach compared to the standard CS and STP-CS approaches. The source code of our experiments can be found at https://github.com/QQ-SDU/DK-STP-CS.

Through rigorous theoretical analysis and extensive experiments, we demonstrate that DK-STP-CS not only outperforms traditional CS and STP-CS methods in terms of PSNR and visual quality but also exhibits greater robustness to noise and adaptability to different measurement matrices. For images or continuous signals, this method can significantly reduce the usage of storage space and improve the quality of the reconstructed signal. This work thus represents a significant step toward practical and efficient compressed sensing systems for next-generation signal processing applications.

1.4 Organization of the paper

The remainder of this paper is organized as follows. Section 2 provides the problem formulation. Section 3 presents the theoretical framework of DK-STP-CS, including formal proofs and the reconstruction errors analysis. Section 4 presents extensive experimental results comparing reconstruction performance across diverse image datasets, sampling rates, and parameter configurations. Finally, Section 5 concludes the paper with insights into future research directions.

2 Problem formulation

In some applications, a time-varying vector $\mathbf{x} \in \mathbb{R}^n$ needs to be transmitted (at some sampling rate) to a destination. A direct transmission would incur enormous resource consumption when the size of $\mathbf{x}$ is large. Therefore, it is convenient to design a constant matrix $\mathbf{A} \in \mathcal{M}_{m\times n}$ $(m \ll n)$ to generate a lower dimensional vector $\mathbf{y} \in \mathbb{R}^m$, with $\mathbf{y} = \mathbf{A}\mathbf{x}$, to be transmitted instead of $\mathbf{x}$. Then, at the destination, the vector $\mathbf{x}$ should be recovered from the transmitted signal $\mathbf{y}$ and the matrix $\mathbf{A}$ which is transmitted once. We refer to $\mathbf{x}$ as the input signal and $\mathbf{y}$ as the output signal. The framework consists of three key components.

• **Compression**: Given an input signal $\mathbf{x} \in \mathbb{R}^n$, find a measurement matrix $\mathbf{A} \in \mathcal{M}_{m\times n}$ $(m \ll n)$, leading to the compressed vector $\mathbf{y} \in \mathbb{R}^m$, such that

$$\mathbf{y} = \mathbf{A}\mathbf{x}.$$

For non-sparse $\mathbf{x}$ with sparsity basis Θ, one has $\mathbf{x} = \boldsymbol{\Theta}\mathbf{s}$, where $\mathbf{s}$ is a sparse signal where most components of the vector are zero. The sensing matrix is given by $\boldsymbol{\Psi} = \mathbf{A}\Theta$. For sparse signals $\mathbf{x}$, the sensing matrix is given by $\boldsymbol{\Psi} = \mathbf{A}$. Therefore,

$$\mathbf{y} = \mathbf{A}\boldsymbol{\Theta}\mathbf{s} = \boldsymbol{\Psi}\mathbf{s}.$$

• **Transmission**: Transmission of the compressed signal $\mathbf{y}$ and the measurement matrix $\mathbf{A}$.

• **Reconstruction**: At the arrival site, we recover the signal $\hat{\mathbf{x}}$ (an approximate of the signal $\mathbf{x}$) through optimization algorithms. We solve an approximate problem formulated as follows:

$$\min_{\mathbf{s}} \|\mathbf{s}\|_1 \quad \text{subject to} \quad \mathbf{y} = \boldsymbol{\Psi}\mathbf{s},$$

and obtain the reconstructed signal $\hat{\mathbf{x}} = \Theta\mathbf{s}$.

In previous work [18], STP was innovatively introduced into compressed sensing, which changed the measurement matrix in the framework.

• **Compression**: Given an input signal $\mathbf{x} \in \mathbb{R}^p$, find a measurement matrix $\mathbf{A} \in \mathcal{M}_{m\times n}$ $(m \ll n)$ and n being a factor of p (i.e., $n \mid p$), leading to the compressed vector $\mathbf{y} \in \mathbb{R}^{m\cdot p/n}$, such that

$$\mathbf{y} = \mathbf{A} \ltimes \mathbf{x} = (\mathbf{A} \otimes \mathbf{I}_{p/n})\mathbf{x}.$$

For non-sparse $\mathbf{x}$ with sparsity basis Θ, one has $\mathbf{x} = \Theta\mathbf{s}$, where $\mathbf{s}$ is a sparse signal. The equivalent sensing matrix is given by $\boldsymbol{\Psi} = (\mathbf{A} \otimes \mathbf{I}_{p/n})\Theta$. For sparse signals $\mathbf{x}$, the equivalent sensing matrix is $\boldsymbol{\Psi} = \mathbf{A} \otimes \mathbf{I}_{p/n}$. Therefore,

$$\mathbf{y} = (\mathbf{A} \otimes \mathbf{I}_{p/n})\Theta\mathbf{s} = \boldsymbol{\Psi}\mathbf{s}.$$

• **Transmission**: Transmission of the compressed signal $\mathbf{y}$ and the measurement matrix $\mathbf{A}$ (which has lower storage requirements compared to traditional CS).

• **Reconstruction**: At the receiver, we recover the signal $\hat{\mathbf{x}}$ through parallel reconstruction algorithms. The reconstruction can be transformed into p/n independent CS problems:

$$\min_{\mathbf{s}^i} \|\mathbf{s}^i\|_1 \quad \text{subject to} \quad \mathbf{y}^i = \mathbf{A}\mathbf{s}^i, \quad \text{for } i = 1, 2, \ldots, p/n,$$

where $\mathbf{y}^i$ are sub-vectors of $\mathbf{y}$. The final reconstructed signal is obtained by combining all $\mathbf{s}^i$ through vectorization: $\hat{\mathbf{x}} = \Theta \cdot \mathrm{vec}([\mathbf{s}^1, \mathbf{s}^2, \ldots, \mathbf{s}^{p/n}]^\top)$.

In practical applications, conventional measurement matrices often require substantial memory storage, which increases transmission costs. To address this problem, we propose a special semi-tensor product called the dimension-keeping semi-tensor product to design the measurement matrix $\mathbf{A}$. In this way, we only need to transmit a smaller measurement matrix to achieve the goal of reconstruction. This significantly reduces the bandwidth cost occupied during transmission and improves the reconstruction quality to a certain extent.

3 Proposed method

In Subsection 3.1, we formalize the algebraic foundation by introducing the DK-STP and its weighted variant, generalizing conventional matrix multiplication to dimension-mismatched cases. Building upon this mathematical groundwork, we then present the novel DK-STP-CS model, incorporating intra-group correlation and inter-group incoherence to enhance sensing matrix design in Subsection 3.2. Finally, a comprehensive error analysis is conducted, decomposing the total reconstruction error into three interpretable components and providing both theoretical bounds and empirical validation in Subsection 3.3.

3.1 Dimension-keeping semi-tensor product

First, we introduce the definition of STP, which is a matrix multiplication across dimensions. When the dimension of the matrix does not meet the traditional matching conditions, it can also be calculated.

Definition 1 ([17, 24]). Let $\mathbf{A} \in \mathcal{M}_{m\times n}$ and $\mathbf{B} \in \mathcal{M}_{p\times q}$, and $t = \mathrm{lcm}(n, p)$ be the least common multiple of n and p. The STP of $\mathbf{A}$ and $\mathbf{B}$, denoted by $\mathbf{A} \ltimes \mathbf{B}$, is defined as

$$\mathbf{A} \ltimes \mathbf{B} := (\mathbf{A} \otimes \mathbf{I}_{t/n})(\mathbf{B} \otimes \mathbf{I}_{t/p}), \tag{7}$$

where $\otimes$ is the Kronecker product and $\mathbf{I}_n$ represents the n-th order identity matrix.

DK-STP is another form of STP, which is expanded from the identity matrix to a row vector with elements of 1. Let $\mathbf{1}_n \in \mathbb{R}^n$ denote an n-dimensional column vector with all entries equal to one.

Definition 2 ([25]). The DK-STP of $\mathbf{A}$ and $\mathbf{B}$ is expressed as follows:

$$\mathbf{A} \rtimes \mathbf{B} := (\mathbf{A} \otimes \mathbf{1}_{t/n}^{\top})(\mathbf{B} \otimes \mathbf{1}_{t/p}), \tag{8}$$

where $\mathbf{A} \in \mathcal{M}_{m\times n}, \mathbf{B} \in \mathcal{M}_{p\times q}, t = \mathrm{lcm}(n, p)$.

Definition 3 ([25]). Let $\mathbf{A} \in \mathcal{M}_{m\times n}, \mathbf{B} \in \mathcal{M}_{p\times q}, t = \mathrm{lcm}(n, p)$. Then the weighted DK-STP is defined as

$$\mathbf{A} \rtimes_w \mathbf{B} := (\mathbf{A} \otimes \boldsymbol{\varepsilon}_{t/n}^{\top})(\mathbf{B} \otimes \boldsymbol{\varepsilon}_{t/p}), \tag{9}$$

where $\boldsymbol{\varepsilon}_n := \frac{1}{\sqrt{n}}\mathbf{1}_n, \mathbf{A} \rtimes_w \mathbf{B} \in \mathcal{M}_{m\times q}$.

The weighted form of DK-STP is adopted to ensure energy preservation and mathematical consistency with conventional compressed sensing theory. The normalization factor $\frac{1}{\sqrt{n}}$ maintains stable variance in the measurement process and enables the sensing matrix to better satisfy RIP conditions, thereby enhancing reconstruction performance, particularly in noisy environments. So in the rest of the paper, we use $\rtimes$ to represent $\rtimes_w$.

Remark 1. All matrix operations in Definitions 1–3 degenerate to the traditional matrix product when the dimensionality compatibility is satisfied. So they can be regarded as an extended form of the traditional matrix product. In Definition 3, the number of rows of matrix $\mathbf{A}$ and the number of columns of matrix $\mathbf{B}$ determine the dimensions of the resulting product matrix.

3.2 Dimension-keeping STP based compressed sensing

DK-STP enables the dimension expansion of the measurement matrix $\mathbf{A}$, thus allowing us to transmit a smaller measurement matrix $\hat{\mathbf{A}}$ compared to traditional compressed sensing while still achieving signal reconstruction. In this section, we enhance the traditional CS measurement matrix by integrating the DK-STP framework, thereby developing the DK-STP-CS model proposed in this work.

Given a measurement matrix $\mathbf{A} \in \mathcal{M}_{m\times n}$, an input signal $\mathbf{x} \in \mathbb{R}^p$, and a compressed signal $\mathbf{y} \in \mathbb{R}^m$ $(m \ll p)$, we want to use DK-STP to optimize the measurement matrix $\mathbf{A}$ to achieve the compression of compressed sensing. The following describes the process of applying the DK-STP to matrix $\mathbf{A}$ and signal $\mathbf{x}$ to derive the enhanced measurement matrix and the compressed signal $\mathbf{y}$,

$$\mathbf{y} = \mathbf{A} \rtimes \mathbf{x} = (\mathbf{A} \otimes \boldsymbol{\varepsilon}_{t/n}^{\top})(\mathbf{x} \otimes \boldsymbol{\varepsilon}_{t/p}), \quad t = \mathrm{lcm}(n, p). \tag{10}$$

In order to reduce the number of measurements, we choose n to be a factor of p and express its ratio as $\gamma = \frac{p}{n}$. Given the above assumptions, the formula can be expressed as

$$\mathbf{y} = (\mathbf{A} \otimes \boldsymbol{\varepsilon}_{\gamma}^{\top})\mathbf{x}. \tag{11}$$

When $\gamma = 1$, DK-STP-CS degenerates into traditional CS. It indicates that DK-STP-CS is an extended form of CS, which can reduce the size of the measurement matrix and realize the role of compressed sensing. Compressed sensing usually processes a sparse signal $\mathbf{x}$ or writes $\mathbf{x}$ in sparse form under some sparse basis. Below we uniformly treat $\mathbf{x}$ as k-sparse, that is l_0 norm:

$$k = \|\mathbf{x}\|_0 .$$

If a vector $\mathbf{x}$ has only k non-zero elements, then we call it k-sparse, represented by $\mathbf{x} \in \sum_k$.

The measurement matrix needs to meet RIP conditions and incoherence, so we use $\mathbf{A} \otimes \boldsymbol{\varepsilon}_{\gamma}^{\top}$ instead of $\mathbf{A}$ as the measurement matrix here. Next we will show that this operation is reasonable and give the relevant theoretical proof.

To establish the theoretical foundation for signal recovery within the DK-STP-CS framework, we now analyze two fundamental properties of the sensing matrix—Spark and Coherence. These properties provide crucial insights into the uniqueness of sparse solutions and the stability of the reconstruction process, thereby validating the feasibility of our proposed approach.

3.2.1 *Spark*

To further analyze the sparse recovery capability of the measurement matrix, we introduce the concept of "Spark", which characterizes the minimal linear dependence among the columns of a matrix, thereby providing a theoretical basis for the uniqueness of sparse solutions in the subsequent analysis.

Definition 4 ([7])**.** The spark of a given matrix $\mathbf{A}$ is the smallest number of columns from $\mathbf{A}$ that are linearly dependent.

To better handle signal representation under the group structure, we define a new vector transformation that sums the original signal within groups, forming a new compressed representation. This paves the way for the subsequent analysis of intra-group correlation.

Definition 5. If $\mathbf{x} \in \mathbb{R}^p$, then $\mathbf{x}^\gamma \in \mathbb{R}^n$ is given by

$$\mathbf{x}^\gamma := \left(\sum_{i=1}^{i=\gamma} x_i, \sum_{i=\gamma}^{i=2\gamma} x_i, \cdots, \sum_{i=(n-1)\gamma}^{i=n\gamma} x_i \right), \tag{12}$$

where x_i stands for the i-th element in $\mathbf{x}$.

The definition above means that the consecutive elements of $\mathbf{x}$ are grouped and summed to produce a new $\mathbf{x}^\gamma$. If $\gamma = 2$, then

$$\mathbf{x}^2 = (x_1 + x_2, x_3 + x_4, \cdots, x_{n-1} + x_n). \tag{13}$$

The following Lemma states that when the sparsity level is sufficiently low, the measurement equation has at most one sparse solution.

Lemma 1 ([7])**.** If $k < \frac{spark(\mathbf{A})}{2}$, then for each $\mathbf{y} \in \mathbb{R}^m$ there exists at most one signal $\mathbf{x} \in \sum_k$ such that $\mathbf{y} = \mathbf{A}\mathbf{x}$.

From Lemma 1, one can obtain the following corollary.

Corollary 1. If $k < \frac{spark(\mathbf{A})}{2}$, then for each $\mathbf{y} \in \mathbb{R}^m$ there exists at most one signal $\mathbf{x}^\gamma \in \sum_k$ such that $\mathbf{y} = \frac{1}{\sqrt{\gamma}}\mathbf{A}\mathbf{x}^\gamma$.

Proof. This is easily obtained by Lemma 1.

The use of $\mathbf{x}^\gamma$ here is equivalent to treating some variable sum of the original vector as a new component. So back to our new measurement matrix which is $\mathbf{A} \otimes \boldsymbol{\varepsilon}_\gamma^\top$, we find $\text{spark}(\mathbf{A} \otimes \boldsymbol{\varepsilon}_\gamma^\top) = 2$. This contradicts our principle of choosing a measurement matrix. We want the spark of the measurement matrix to be as large as possible. We can represent

$$\mathbf{A} \otimes \boldsymbol{\varepsilon}_\gamma^\top = \frac{1}{\sqrt{\gamma}} \begin{bmatrix} a_{11} & \cdots & a_{11} & \cdots & a_{1n} & \cdots & a_{1n} \\ a_{21} & \cdots & a_{21} & \cdots & a_{2n} & \cdots & a_{2n} \\ \vdots & & \vdots & & \vdots & & \vdots \\ a_{n1} & \cdots & a_{n1} & \cdots & a_{nn} & \cdots & a_{nn} \end{bmatrix}. \tag{14}$$

Then it is easy to verify the following equation $(\mathbf{A} \otimes \boldsymbol{\varepsilon}_\gamma^\top)x = \frac{1}{\sqrt{\gamma}}\mathbf{A}\mathbf{x}^\gamma$. So we turned the problem of $\mathbf{y} = (\mathbf{A} \otimes \boldsymbol{\varepsilon}_\gamma^\top)\mathbf{x}$ into $\mathbf{y} = \frac{1}{\sqrt{\gamma}}\mathbf{A}\mathbf{x}^\gamma$. This is different from what we required for spark before. Now that the adjacent elements are related, we choose to deal with the sum value problem of vectors. The converted problem actually goes back to the traditional CS problem.

The following theorem indicates that in the DK-STP-CS framework, there exist sparse solutions for the sampling system under certain conditions.

Theorem 1. If $k < \frac{spark(\mathbf{A})}{2}$, then for each $\mathbf{y} \in \mathbb{R}^m$ there exists one signal $\mathbf{x} \in \sum_k$ such that $\mathbf{y} = \mathbf{A} \rtimes \mathbf{x}$.

Proof. If $k < \frac{spark(\mathbf{A})}{2}$, then $\|\mathbf{x}\|_0 = k$. By Definition 5,

$$\|\mathbf{x}^\gamma\|_0 \leqslant \|\mathbf{x}\|_0 = k,$$

hence we can get at most one signal $\mathbf{x}^\gamma$ by Theorem 1. However, $\mathbf{x}^\gamma$ determines the sum of the continuous components of the original signal $\mathbf{x}$, and cannot determine the specific distribution in the original signal, but for the relatively

smooth vector signal, it can have a good reduction result. It will not cause too much distortion, especially for image signals.

We can obtain a signal $\mathbf{x}$ from $\mathbf{x}^\gamma$ by adopting some distribution principle, such as equalization. But note that this distribution is not unique. In the experiment, the adjacent values are relatively close, and the common sum values are unchanged, but it is not an accurate average distribution.

3.2.2 *Coherence*

In traditional compressed sensing, the coherence $\mu(\mathbf{A})$ of matrix $\mathbf{A}$ is defined as

$$\mu(\mathbf{A}) = \max_{1\leqslant i\neq j\leqslant n} \frac{|\langle \mathbf{a}_i, \mathbf{a}_j\rangle|}{\|\mathbf{a}_i\|_2 \|\mathbf{a}_j\|_2}. \tag{15}$$

This has been pointed out in previous studies $\mu(\mathbf{A}) \in [\sqrt{\frac{n-m}{m(n-1)}}, 1]$ [26, 27]. For matrix $\mathbf{A}\otimes\boldsymbol{\varepsilon}_\gamma^\top$, its coherence $\mu(\mathbf{A}\otimes\boldsymbol{\varepsilon}_\gamma^\top) = 1$. But we want $\mu(\mathbf{A}\otimes\boldsymbol{\varepsilon}_\gamma^\top)$ to be as small as possible. We can solve the above problem by analyzing x^γ.

For any matrix $\mathbf{A}$, $spark(\mathbf{A}) \leqslant 1 + \frac{1}{\mu(\mathbf{A})}$. The following Corollaries provide the relationship between the sparsity of the signal and the coherence of the sensing matrix.

Corollary 2. If $k < \frac{1}{2}(1 + \frac{1}{\mu(\mathbf{A})})$, then for each $\mathbf{y} \in \mathbb{R}^m$ there exists at most one signal $\mathbf{x}^\gamma \in \sum_k$ such that $\mathbf{y} = \frac{1}{\sqrt{\gamma}}\mathbf{A}\mathbf{x}^\gamma$.

Corollary 3. If $k < \frac{1}{2}(1 + \frac{1}{\mu(\mathbf{A})})$, then for each $\mathbf{y} \in \mathbb{R}^m$ there exists one signal $\mathbf{x} \in \sum_k$ such that $\mathbf{y} = \mathbf{A} \rtimes \mathbf{x}$.

From here we can see that the measurement matrix satisfies a certain correlation and can also achieve compressed sensing. We call it intra-group correlation. Next, the definition of intra-group correlation is given.

Definition 6. If the columns of a matrix A are equally divided into n groups such that the column vectors within each group are highly coherent, while the vectors across different groups are mutually incoherent, then the matrix exhibits a structure known as intra-group correlation.

To clarify the above definition, we give a Gaussian random matrix $\mathbf{A}$, which is a matrix with columns incoherence. Then $\mathbf{A}\otimes\boldsymbol{\varepsilon}_\gamma^\top$ is a matrix that satisfies Definition 6, and it can be inferred that there is still a unique solution for $\mathbf{x}^\gamma$ by Corollary 2. This indicates that after the column grouping of the measurement matrix, if the vectors between groups remain uncorrelated while those within groups are correlated, a very good reconstruction effect can still be achieved in terms of images.

When there are few vectors in the group, this correlation actually does not affect us to do compressed sensing, especially in image compressed sensing. This part will be discussed in the following experiment.

3.2.3 *Restricted isometry property*

The following lemma shows us that if the sensing matrix meets the RIP condition, the precise recovery of compressed sensing can be achieved through l_1 optimization.

Lemma 2 ([18])**.** For any p-dimensional vector $\mathbf{x} \in \sum_k$, if the sensing matrix $\mathbf{A}$ satisfies the RIP of order $2k$ with the constant $\delta_{2k}^{\mathbf{A}} < \sqrt{2} - 1$, then the exact recovery in CS model is guaranteed via l_1-minimization.

Furthermore, we will prove that within the DK-STP-CS framework, even when using a measurement matrix with intra-group correlation, the original signal can still be uniquely recovered from the group-summed signal provided certain sparsity conditions are met. The following theorem provides the requirement for the coefficient in the RIP condition.

Theorem 2. If $\mathbf{A}$ satisfies the RIP of order $2k$ with constant $\delta_{2k}^{\mathbf{A}} < \sqrt{2}-1$, then the exact recovery for $\mathbf{y} = \frac{1}{\sqrt{\gamma}}\mathbf{A}\mathbf{x}^\gamma$ is guaranteed via l_1-minimization.

Proof. If $\mathbf{A}$ satisfies the RIP of order $2k$ with constant $\delta_{2k}^{\mathbf{A}}$, then

$$(1-\delta_{2k}^{\mathbf{A}})\|\mathbf{x}\|_2^2 \leqslant \|\mathbf{A}\mathbf{x}\|_2^2 \leqslant (1+\delta_{2k}^{\mathbf{A}})\|\mathbf{x}\|_2^2. \tag{16}$$

Taking $\mathbf{x} = \frac{1}{\sqrt{\gamma}}\mathbf{x}^\gamma$, we find

$$(1-\delta_{2k}^{\mathbf{A}})\|\mathbf{x}^\gamma\|_2^2 \leqslant \|\mathbf{A}\mathbf{x}^\gamma\|_2^2 \leqslant (1+\delta_{2k}^{\mathbf{A}})\|\mathbf{x}^\gamma\|_2^2. \tag{17}$$

By Lemma 2, the theorem has been proven.

3.3 Error analysis

Reconstruction error analysis is an important part, as it is directly related to the reconstruction performance and serves as a key indicator of the effectiveness of the method. This subsection analyzes the reconstruction error in the proposed compressed sensing-based dimension-keeping semi-tensor product method, which is attributed to three fundamental sources: the original signal error, the compressed sensing error, and the distribution error, thereby providing a fundamental explanation of the error causes and highlighting the superiority of our method. To this end, some symbol definitions are provided.

- x^* represents the reconstructed signal for original signal $\mathbf{x}$.
- x_i represents each component of the signal $\mathbf{x}$.
- x_i^* represents each component of the signal $\mathbf{x}^*$.
- $\mathbf{x}^{\gamma*}$ represents the sum of each component of the reconstructed signal $\mathbf{x}^*$.

$$\mathbf{x}^{\gamma*} := \left(\sum_{i=1}^{i=\gamma} x_i^*, \sum_{i=\gamma}^{i=2\gamma} x_i^*, \cdots, \sum_{i=(n-1)\gamma}^{i=n\gamma} x_i^* \right). \tag{18}$$

- $\frac{\mathbf{x}^{\gamma}}{\gamma}$ and $\frac{\mathbf{x}^{\gamma*}}{\gamma}$ represent the average number. Their dimensions are different from the original signal $\mathbf{x}$, so each component is repeated γ times to obtain $\bar{\mathbf{x}}$ and $\bar{\mathbf{x}^*}$ with the same dimension as the original signal x. Such as

$$\bar{\mathbf{x}} := \left(\underbrace{\sum_{i=1}^{i=\gamma} \frac{x_i}{\gamma}, \cdots, \sum_{i=1}^{i=\gamma} \frac{x_i}{\gamma}}_{\gamma}, \underbrace{\sum_{i=\gamma}^{i=2\gamma} \frac{x_i}{\gamma}, \cdots, \sum_{i=\gamma}^{i=2\gamma} \frac{x_i}{\gamma}}_{\gamma}, \cdots, \sum_{i=(n-1)\gamma}^{i=n\gamma} \frac{x_i}{\gamma} \right). \tag{19}$$

Based on the above symbolic explanations, a norm estimation of the reconstructed signal and the original signal is provided. This helps us analyze some factors that affect the error.

Theorem 3. For the estimation of $\|\mathbf{x}^* - \mathbf{x}\|_2$, the following norm inequality holds:

$$\|\mathbf{x}^* - \mathbf{x}\|_2 \leqslant \|\mathbf{x}^* - \bar{\mathbf{x}}\|_1 + \|\mathbf{x}^{\gamma} - \mathbf{x}^{\gamma*}\|_1 + \|\bar{\mathbf{x}} - \mathbf{x}\|_1 .$$

Proof. Note that

$$\begin{aligned} \|\mathbf{x}^* - \mathbf{x}\|_1 &= \|\mathbf{x}^* - \bar{\mathbf{x}^*} + \bar{\mathbf{x}^*} - \bar{\mathbf{x}} + \bar{\mathbf{x}} - \mathbf{x}\|_1 \\ &\leqslant \|\mathbf{x}^* - \bar{\mathbf{x}^*}\|_1 + \|\bar{\mathbf{x}^*} - \bar{\mathbf{x}}\|_1 + \|\bar{\mathbf{x}} - \mathbf{x}\|_1 \\ &= \|\mathbf{x}^* - \bar{\mathbf{x}} + \bar{\mathbf{x}} - \bar{\mathbf{x}^*}\|_1 + \|\bar{\mathbf{x}^*} - \bar{\mathbf{x}}\|_1 + \|\bar{\mathbf{x}} - \mathbf{x}\|_1 \\ &\leqslant \|\mathbf{x}^* - \bar{\mathbf{x}}\|_1 + 2\|\bar{\mathbf{x}} - \bar{\mathbf{x}^*}\|_1 + \|\bar{\mathbf{x}} - \mathbf{x}\|_1 \\ &= \|\mathbf{x}^* - \bar{\mathbf{x}}\|_1 + \|\mathbf{x}^{\gamma} - \mathbf{x}^{\gamma*}\|_1 + \|\bar{\mathbf{x}} - \mathbf{x}\|_1 . \end{aligned}$$

Then it follows that

$$\|\mathbf{x}^* - \mathbf{x}\|_2 \leqslant \|\mathbf{x}^* - \mathbf{x}\|_1 \leqslant \|\mathbf{x}^* - \bar{\mathbf{x}}\|_1 + \|\mathbf{x}^{\gamma} - \mathbf{x}^{\gamma*}\|_1 + \|\bar{\mathbf{x}} - \mathbf{x}\|_1 .$$

From Theorem 3, the l_2 norm of this reconstruction error is restricted by three terms.

- Distribution error $\|\mathbf{x}^* - \bar{\mathbf{x}}\|_1$.
- Compressed sensing error $\|\mathbf{x}^{\gamma} - \mathbf{x}^{\gamma*}\|_1$.
- Original signal error $\|\bar{\mathbf{x}} - \mathbf{x}\|_1$.

Below, we will conduct data analysis on these three types of errors, respectively, through three experimental images.

3.3.1 *Original signal error*

For the original signal error, the element values in the signal should not deviate too much from the mean of their adjacent elements. This can ensure that the error is as small as possible. In simple terms, the signal needs to be as continuous as possible and avoid sudden and excessive fluctuations. For common signal sources, the relative continuity of image signals is relatively strong, and the difference in adjacent pixel values is not significant, which is quite suitable for us to select the original signal here. So next, we, respectively, select the truncated parts from different images as the original signals to calculate the magnitude of this error.

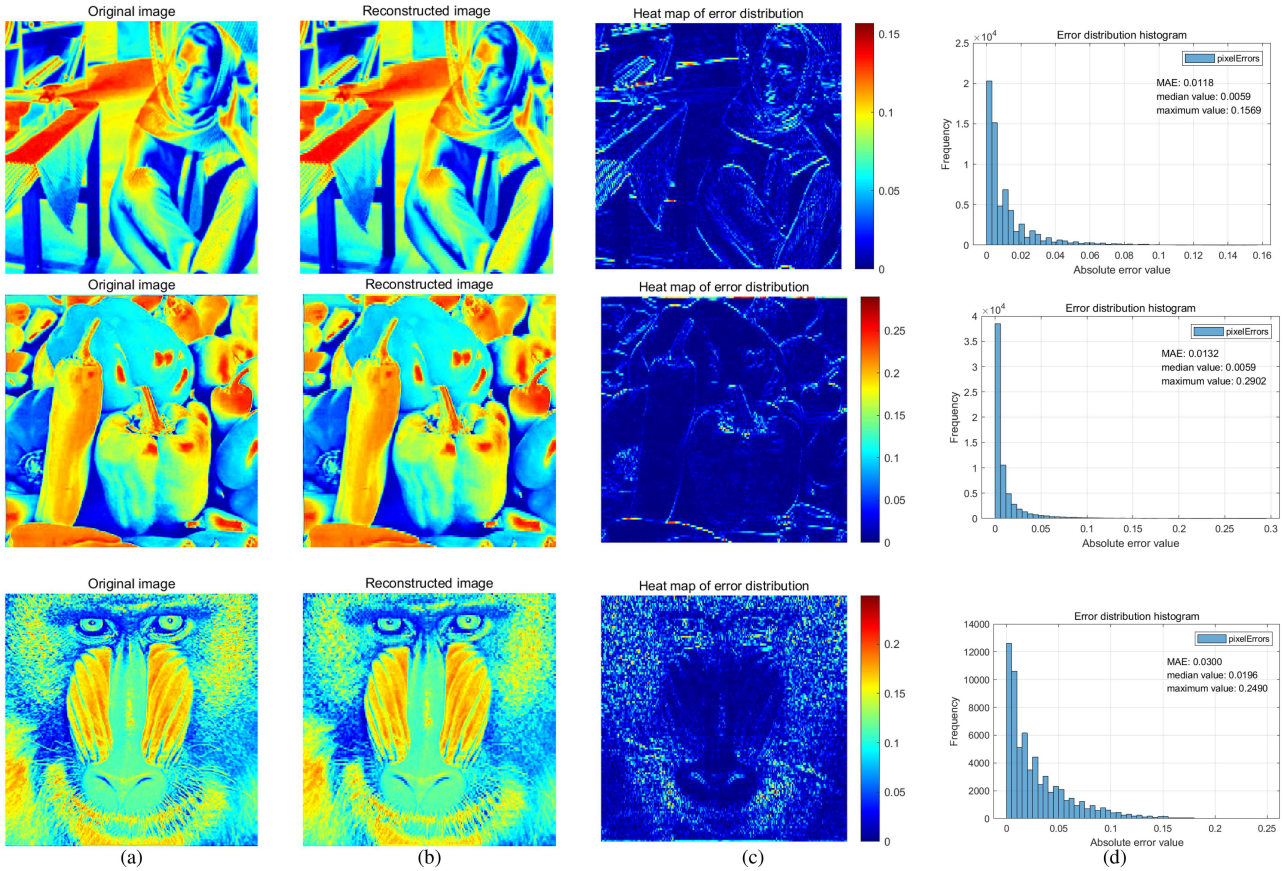

Figure 1 (Color online) Comparison of reconstruction heat maps of three test images (Barbara, Pepper, and Baboon). (a) Original heat map; (b) mean reconstruction image; (c) heat map of the error distribution between the original and reconstructed images; (d) histogram of the error frequency distribution.

In image processing, the l_1 norm error is usually used to calculate the MAE value for comparison. The mean absolute error (MAE) is defined as follows:

$$\mathrm{MAE} = \frac{1}{N}\sum_{i=1}^{N}|X_i - Y_i|,$$

where X_i represents the i-th element value of the original signal X and Y_i represents the i-th element value of the reconstructed signal Y.

The calculation of the mean signal $\bar{x}$ for three natural images is called the reconstructed image. We calculate its heat map of error distribution to observe the overall error distribution of the image, and draw its frequency distribution histogram to help analyze the error.

As shown in Figure 1, the original signal error of the natural image is relatively small, and the places with larger errors occur at the boundaries, which account for a relatively small proportion of the overall error. It can be seen from the frequency distribution histogram that the errors of most pixels are concentrated around 0, which ensures that the error of the original signal is relatively small.

3.3.2 *Compressed sensing error*

The compressive sensing error here represents the error of the signal composed of the sum values of adjacent pixels, which indicates that we have shifted from the reconstruction of the original signal to the reconstruction of signals with fewer sum values. To some extent, this reduces the compression ratio, which will make the reconstruction of the sum value signal more accurate. The reduced error here is greater than the two types of increased errors, so it makes the effect of image reconstruction better. In Figure 2, five 64×64 pixel blocks are randomly selected from different images for compressive sensing. The compression ratio ranges from 5% to 100%, increasing by 5% each time. The average MAE value of these five pixel blocks is calculated, and the relevant images are drawn. Taking γ

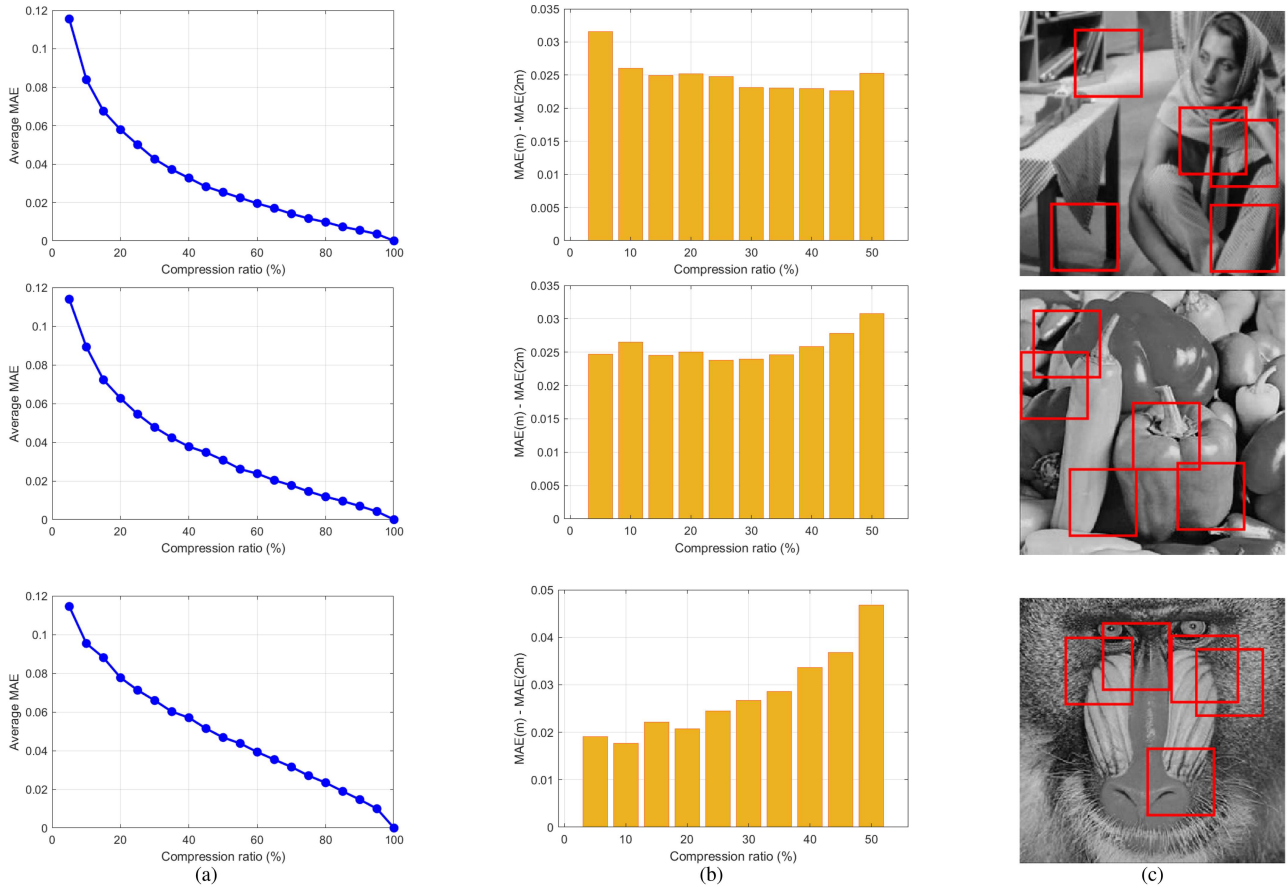

Figure 2 (Color online) Comparison of MAE metrics of three test images (Barbara, Pepper, and Baboon). (a) Average MAE; (b) MAE difference under a compression ratio difference of twice; (c) selected 5 pixel blocks.

equal to 2 as an example, we calculate the change in MAE value when the compression ratio varies by twice and draw a histogram.

It can be seen from the image that when the compression ratio increases by two times, the MAE value has significantly improved. This is also the reason why in DK-STP-CS, the compression ratio of the sum value has been increased while the overall compression ratio remains unchanged. The overall quality of the image was retained at the expense of some details.

3.3.3 *Distribution error*

The essence of the allocation error is that we only recover the sum value signal, but the information on how to allocate the sum value to each element is lost. The loss of local information has made the overall information more accurate. This part of the error is also limited by the error of the original signal. If the error of the original signal of a signal is 0, then we can distribute it evenly. In this way, the distribution error will not occur. In natural images, distribution errors are bound to exist and to some extent depend on the pixel values of the image and the compression ratio. The distribution error curves of the three images are represented in Figure 3.

In terms of overall error analysis, our approach can effectively enhance the overall quality of the image while neglecting some detailed information. Under the premise that the image is large enough, these lost details can be ignored. However, the overall improvement in quality can be clearly felt.

The theoretical foundation of our reconstruction framework is established through rigorous analysis of two critical matrix properties: Spark and Coherence. These metrics collectively ensure the uniqueness of sparse solutions and validate the feasibility of the proposed approach. Specifically, the Spark parameter guarantees solution uniqueness under sparsity constraints, while Coherence quantification governs measurement matrix optimization. Furthermore, the algorithmic implementation is formally presented in Algorithm 1, which outlines the complete reconstruction pipeline.

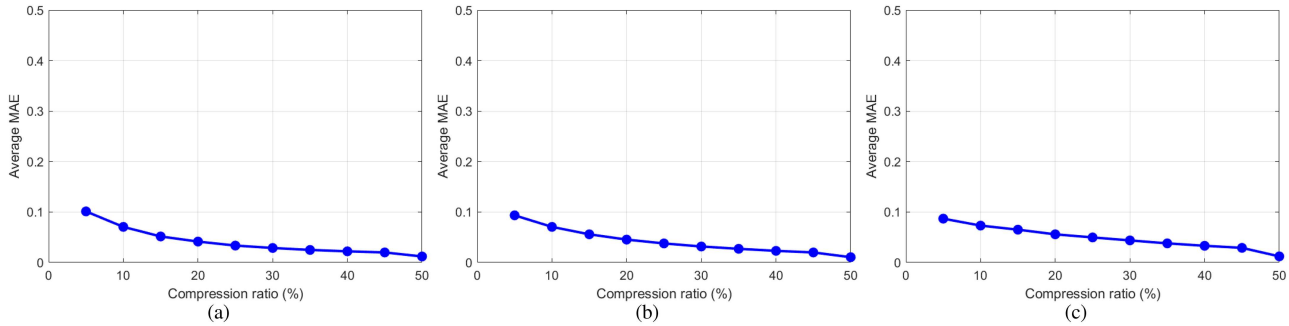

Figure 3 (Color online) Distribution error curves of (a) Barbara, (b) Pepper, and (c) Baboon.

Algorithm 1 DK-STP-CS reconstruction algorithm.

Require: Measurement signal $\mathbf{y} \in \mathbb{R}^m$, sensing matrix $\mathbf{A} \in \mathbb{R}^{m \times \frac{p}{\gamma}}$, parameter γ;
Ensure: Reconstructed image $\mathbf{x} \in \mathbb{R}^p$;
for $i = 1$ to γ **do**
  $x^i \leftarrow (x_{(i-1)\gamma+1} + x_{(i-1)\gamma+2} + \cdots + x_{i\gamma})$;
end for
$\mathbf{X} \leftarrow \left[x^1 \ x^2 \ \cdots \ x^\gamma\right] \in \mathbb{R}^{\frac{p}{\gamma}}$;
$\mathbf{y} = \hat{\mathbf{A}}\mathbf{x} = (\mathbf{A} \otimes \boldsymbol{\epsilon}_\gamma^\top)\mathbf{x} = \frac{1}{\sqrt{\gamma}}\mathbf{A}\mathbf{X}$;
Solve problem:
$\mathbf{X} \leftarrow \arg\min_{\mathbf{z}} \|\mathbf{z}\|_1$ s.t. $\mathbf{A}\mathbf{z} = \mathbf{y}$;
Reshape results:
$\mathbf{x} \leftarrow \mathbf{X}$;
return $\mathbf{x}$;

4 Experimental results and discussions

To assess the reconstruction efficacy of the DK-STP-CS framework, we conducted comparative analyses against standard CS and STP-CS methodologies, employing basis pursuit (BP) as the unified recovery algorithm. Specifically, the performance differentials among DK-STP-CS, STP-CS, and CS were rigorously quantified. Furthermore, we analyzed the time complexity and storage requirements of the DK-STP-CS architecture to evaluate its computational feasibility.

In subsequent experimental validations, the sensing matrix for DK-STP-CS was instantiated as a Gaussian random matrix. The evaluation protocol incorporated visual quality assessments and quantitative metrics, with a focus on image signal recovery tasks. The reconstruction fidelity was measured via the peak signal-to-noise ratio (PSNR), defined as

$$\mathrm{PSNR} = 10 \lg \left[\frac{(MAX_I)^2}{\mathrm{MSE}}\right].$$

In this context, ξ denotes the bit depth per pixel, conventionally set to $\xi = 8$ for standard grayscale images, corresponding to a maximum intensity value of $MAX_I = 2^\xi - 1 = 255$. During subsequent experimental procedures, the PSNR is expressed in dB. The mean squared error (MSE) quantifies the discrepancy between the original image I and the reconstructed image J, formally defined as

$$\mathrm{MSE} = \frac{1}{mn}\sum_{i=0}^{m-1}\sum_{j=0}^{n-1}(I(i,j) - J(i,j))^2,$$

where $m \times n$ represents the image dimensions, and $I(i,j), J(i,j)$ denote pixel intensities at position (i,j) in the original and recovered images, respectively. This metric provides a pixel-wise fidelity assessment critical for evaluating reconstruction accuracy in imaging applications. We take the grayscale image and transform it into a matrix where the elements represent the grayscale value of each pixel. That is, we correspond each image to a matrix, and arrange each column of the matrix in a column in order to obtain a vector signal.

Given a grayscale image represented as matrix $\mathbf{A} \in \mathcal{M}_{m\times n}$, the corresponding vector representation $\mathbf{x} \in \mathbb{R}^{mn}$ can be obtained through column-wise vectorization, expressed as

$$\mathbf{x} = \mathrm{vec}(\mathbf{A}) = [a_{11}, ..., a_{m1}, a_{12}, ..., a_{m2}, ..., a_{1n}, ..., a_{mn}]^\top,$$

where $\mathrm{vec}(\cdot)$ denotes the vectorization operator that stacks matrix columns sequentially.

Table 1 PSNR values using different CS methods in Figure 4.

Methods	Barbara	Pepper	Baboon
CS	32.0151	29.4298	24.3347
STP-CS	30.6257	28.2639	23.9777
DK-STP-CS	34.3620	31.2494	27.2071

4.1 Visual and PSNR comparisons of different images at the same sampling rate

The proposed framework is validated using a standard 256×256 grayscale test image, which is vectorized into $\mathbf{x} \in \mathbb{R}^{65536}$ through column-wise concatenation. Three distinct measurement matrices are implemented for comparative analysis.

- **Conventional CS**: $\mathbf{A}_{CS} \in \mathbb{R}^{m\times n}$ with independent and identically distributed (i.i.d.) Gaussian entries $\mathcal{N}(0,1)$,
- **STP-CS**: $\mathbf{A}_{STP-CS} = \mathbf{A}_{\frac{m}{\gamma}\times\frac{n}{\gamma}} \otimes \mathbf{I}_\gamma$, where $\otimes$ denotes Kronecker product,
- **DK-STP-CS**: $\mathbf{A}_{DK-STP-CS} = \mathbf{A}_{m\times\frac{n}{\gamma}} \otimes \boldsymbol{\varepsilon}_\gamma^\top$, with $\boldsymbol{\varepsilon}_\gamma = \frac{1}{\sqrt{\gamma}}\mathbf{1}_\gamma$,

where $n = 65536$ (original dimension), $m = 32768$ (compressed dimension). The signal sparsity is induced through the discrete cosine transform (DCT) basis Θ, such that $\mathbf{x} = \Theta\mathbf{s}$. This configuration yields a compression ratio $CR = m/n = 0.5$, enabling systematic evaluation of reconstruction fidelity under controlled dimensionality reduction. The hyperparameter $\gamma = p/n$ represents the group size or compression factor at the measurement matrix level, which fundamentally governs the trade-off between resource efficiency and reconstruction fidelity in the DK-STP-CS framework. As defined in the operation $(\mathbf{A} \otimes \boldsymbol{\varepsilon}_\gamma^\top)\mathbf{x} = \frac{1}{\sqrt{\gamma}}\mathbf{A}\mathbf{x}^\gamma$, γ determines how many adjacent elements of the original signal $\mathbf{x} \in \mathbb{R}^p$ are effectively grouped and summed. A larger γ provides greater compression of the measurement matrix, minimizing storage and bandwidth requirements through stronger intra-group correlation and greater reduction in the size of the base measurement matrix $\mathbf{A}$. However, this advantage comes at the cost of increased distribution error, where fine-grained details within each group are lost when only their collective sum is preserved. Conversely, a smaller γ preserves more signal detail but offers diminished reduction in resource overhead. The optimal selection of γ is further influenced by the inherent properties of the target signal: images with large, smooth regions (e.g., Pepper) can tolerate larger γ values as the distribution error remains naturally low, while images rich in high-frequency textures and details (e.g., Baboon) typically require smaller γ values to avoid excessive blurring and preserve critical structural information.

As illustrated in Figure 4, under a compression ratio (CR) of 0.5, which corresponds to sampling only 50% of the original pixels, the reconstructed images exhibit distinct performance variations across methodologies. Visual inspection reveals that conventional CS and STP-CS frameworks introduce substantial noise artifacts, significantly impairing image recognition fidelity. In contrast, the proposed DK-STP-CS architecture effectively suppresses noise contamination, as evidenced by smoother texture regions and reduced granular distortions. This improvement aligns with the inherent mechanism of DK-STP-CS: during reconstruction, adjacent pixel blocks are restored holistically through the dimension-keeping semi-tensor product operation, thereby mitigating abrupt intensity fluctuations between neighboring regions. However, edge preservation remains a relative limitation of DK-STP-CS. Quantitative analysis of Figure 4(d) demonstrates that while the method achieves superior intra-block coherence, it occasionally introduces mild aliasing artifacts along high-frequency edges compared to CS and STP-CS baselines. This trade-off between noise suppression and edge sharpness reflects the inter-group correlation characteristics embedded in the DK-STP measurement matrix design, as theoretically established in Subsection 3.2. The observed performance dichotomy underscores the method's suitability for applications prioritizing homogeneous region fidelity over fine edge reconstruction.

The superior visual performance of DK-STP-CS, as demonstrated in Figure 4, is further substantiated through rigorous quantitative analysis. To objectively evaluate reconstruction quality, we employ the PSNR metric and conduct systematic comparisons across 50 independent trials. For each experiment, distinct Gaussian random matrices were regenerated to eliminate bias from measurement matrix initialization, ensuring statistical robustness in performance evaluation. The resultant PSNR trajectories, aggregated in Figure 5, reveal consistent superiority of DK-STP-CS over conventional CS and STP-CS baselines. Specifically, the DK-STP-CS curves occupy the uppermost position across all tested images, with mean PSNR improvements of 2.35, 1.82, and 2.87 dB, respectively, as quantified in Table 1. These statistically significant enhancements validate the method's efficacy in preserving both global structural integrity and local texture details.

The variance in improvement magnitude across images correlates strongly with inherent signal characteristics. For instance, the Baboon image, characterized by its high-frequency edge components and intricate texture patterns,

Figure 4 Recovered images by different CS models. (a) Original images (256×256); (b) results of the CS method; (c) results of the STP-CS method; (d) results of the DK-STP-CS method. In the measurement process, the Gaussian random matrix is taken as the measurement matrix. The recovery method is BP.

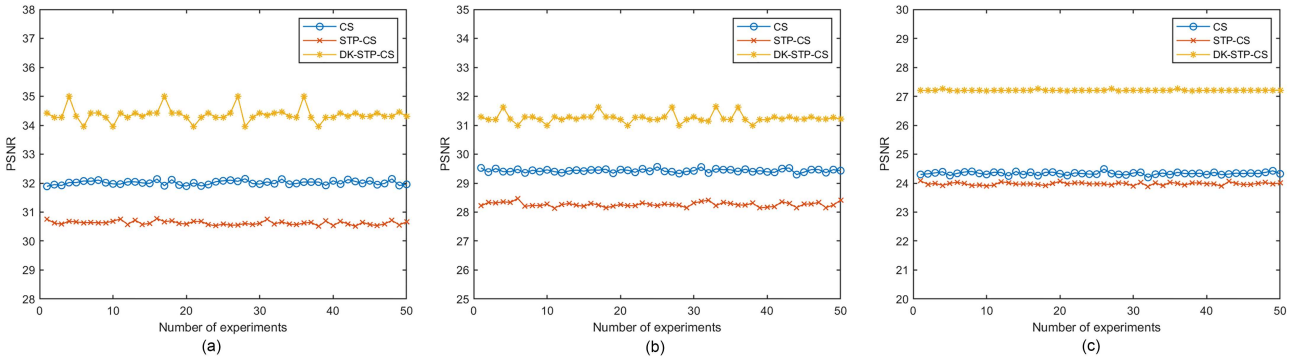

Figure 5 (Color online) PSNR values of (a) Barbara, (b) Pepper, and (c) Baboon corresponding to the 50 different experiments. In the measurement process, the Gaussian random matrix is taken as the measurement matrix. The recovery method is BP.

demonstrates the most significant PSNR improvement with DK-STP-CS (27.21 dB) compared to conventional CS (24.33 dB). This result highlights the method's enhanced capacity to mitigate noise propagation in structurally complex regions. In contrast, the Pepper image—with its predominantly smooth texture—achieves a moderate yet consistent PSNR improvement of 31.25 dB compared to 29.43 dB for conventional CS. This behavior aligns with the inter-group correlation mechanism (Subsection 3.2), which inherently optimizes reconstruction fidelity for piecewise-constant signal components. This performance dichotomy aligns with theoretical predictions in Subsection 3.3 regarding RIP-constrained recovery guarantees. Collectively, these results confirm that DK-STP-CS achieves dual objectives: enhancing reconstruction fidelity for recognition-critical features while maintaining computational tractability.

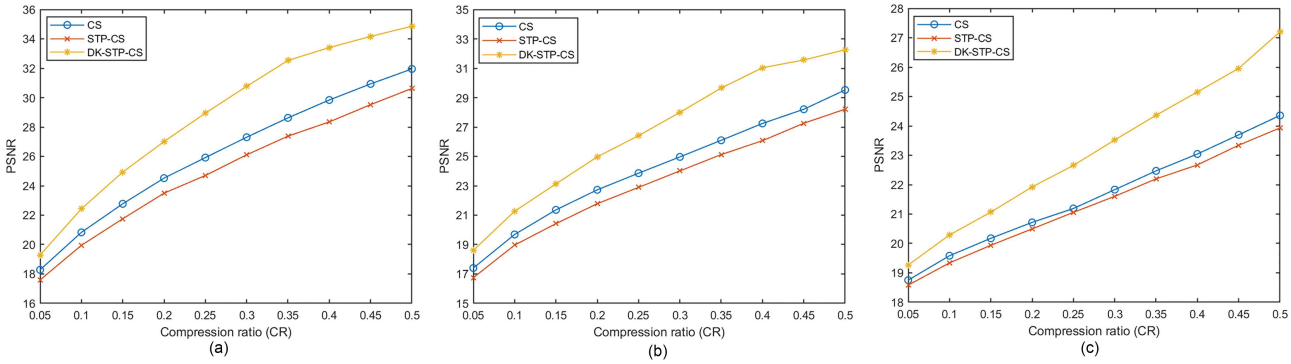

Figure 6 (Color online) PSNR values of (a) Barbara, (b) Pepper, and (c) Baboon across different sampling rates for each method. In the measurement process, the Gaussian random matrix is taken as the measurement matrix. The recovery method is BP.

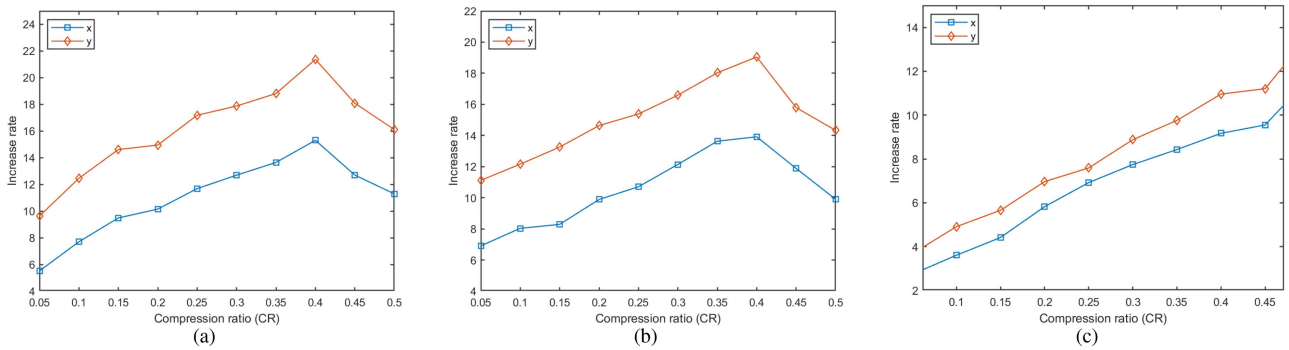

Figure 7 (Color online) The increase rate curves of DK-STP-CS compared to CS and STP-CS. (a) Barbara; (b) Pepper; (c) Baboon. x represents the comparison with STP-CS while y represents the comparison with CS.

4.2 The performance of various methods under different sampling rates

In the aforementioned experiments, the sampling rate was consistently fixed at 0.5. Next, we analyze the PSNR curves of each method under different sampling rates.

Here, we conducted experiments on three images at different sampling rates. In Figure 6, the x-axis represents the sampling rate, ranging from 0.05 to 0.50 with intervals of 0.05. As the sampling rate increases, the PSNR values of all three methods also increase. We can observe that the PSNR value curves vary across different images.

As illustrated in Figure 6, the DK-STP-CS curve lies above the other two curves, indicating a significant improvement in image reconstruction quality regardless of the sampling rate. As x approaches 0.50, the extent of improvement becomes more pronounced compared to lower sampling rates. In order to compare the increase rate, we calculated the increase rate for each group of data separately and plotted it in Figure 7. In Figure 7, the horizontal axis represents the sampling rate, while the vertical axis represents the increase rate. Curve x corresponds to the comparison with STP-CS, and curve y corresponds to the comparison with CS. Here we can observe that the growth rate curves x and y are similar for the same image. For Figures 7(a) and (b), the maximum growth rate occurs at a sampling rate of 0.4, while for Figure 7(c), the maximum growth rate is observed at a sampling rate of 0.5, which is meaningful for our subsequent efforts to improve the reconstruction of image quality. Moreover, the increase rate varies across different images, which depends on the inherent characteristics of the images themselves.

4.3 Comparison of different methods under the influence of noise

During signal transmission, it is inevitable that some noise will be introduced. To some extent, this noise can affect the reconstruction of the original image, making it essential to analyze image reconstruction under the influence of noise. Below, we will separately add a certain level of Gaussian noise to CS, STP-CS and DK-STP-CS models before performing reconstruction. This will allow us to compare the impact of noise on the performance of these different methods. The introduction of noise here refers to replacing each element a_{ij} of the grayscale matrix with $\hat{a}_{ij}$, where $\hat{a}_{ij}$ is defined as follows:

$$\hat{a}_{ij} = a_{ij} + \sigma_{ij}.$$

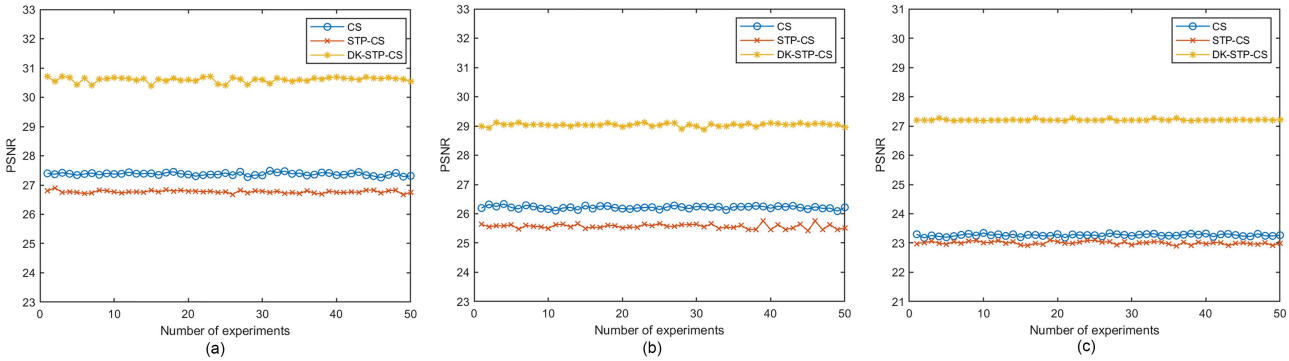

Figure 8 (Color online) PSNR values of (a) Barbara, (b) Pepper, and (c) Baboon corresponding to the 50 different experiments under the influence of noise. In the measurement process, the Gaussian random matrix is taken as the measurement matrix. The recovery method is BP.

Table 2 PSNR values of different CS methods in Figure 8.

Method	Barbara	Pepper	Baboon
CS	27.3749	26.2154	23.2677
STP-CS	26.7690	25.5691	23.0023
DK-STP-CS	30.6024	28.6355	27.2095

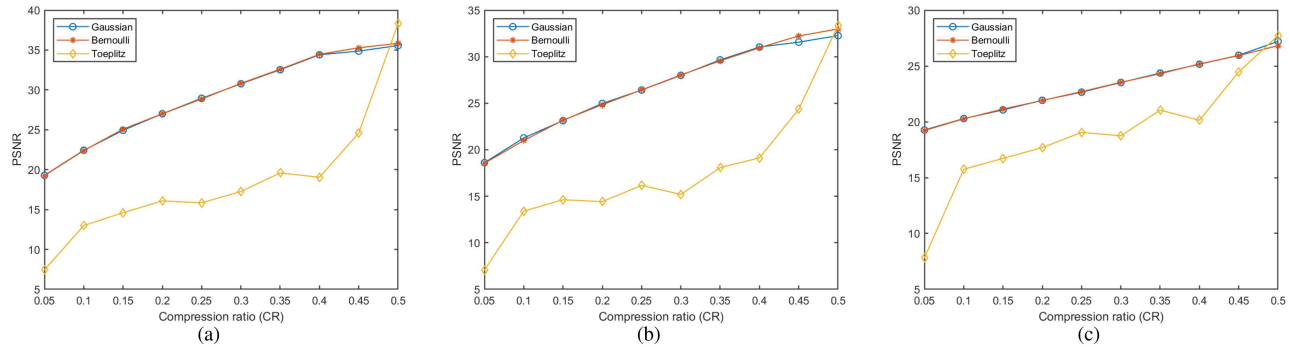

Figure 9 (Color online) PSNR values of (a) Barbara, (b) Pepper, and (c) Baboon across different measurement matrices for each method. The recovery method is BP.

Here, σ is a random variable following the distribution with $E[\sigma] = 0$ and $D[\sigma] = 0.001$. After adding noise to the original image to approximate the vector signal affected by noise during transmission, we conducted 50 repeated experiments for each of the aforementioned three images. Here, the measurement matrix A is taken as a generated Gaussian random matrix. We plotted the experimental data to compare and analyze the PSNR values against the number of experiments, as shown in Figure 8. Additionally, we provide the mean values for the data in the graph, as shown in Table 2.

From Table 2, it is evident that the DK-STP-CS method significantly enhances the quality of reconstructed images even in the presence of noise interference. This demonstrates its robustness and effectiveness in handling noisy conditions, making it a reliable approach for improving image reconstruction under such challenging scenarios.

4.4 Further comparative analysis under different measurement matrices

In the DK-STP-CS, the reconstruction results are influenced by many factors. For instance, the choice of the measurement matrix plays a critical role. In the aforementioned experiments, we consistently employed a Gaussian matrix as the measurement matrix. Next, we will replace the Gaussian matrix with other types of measurement matrices and compare the reconstruction performance under different sampling rates. This comparison will facilitate the selection of the most effective measurement matrix for practical applications. The experimental results are shown in Figure 9.

We select the Gaussian matrix, Bernoulli matrix, and Toeplitz matrix as the measurement matrices. Experiments are conducted on each of the three images using these three measurement matrices. Comparisons of reconstruction performance are conducted under different compression ratios. We still set $\gamma = 2$.

Table 3 Comparison of CS, STP-CS and DK-STP-CS methods in terms of storage space and sampling complexity.

Type	Sampling model	Storage matrix	Sampling complexity	Storage space
CS	$y = \Phi_1 x$	$\Phi_1 \in \mathbb{R}^{m \times N}$	mN	mN
STP-CS	$y = \Phi_2 \ltimes x$	$\Phi_2 \in \mathbb{R}^{\frac{m}{t} \times \frac{N}{t}}$	$\frac{mN}{t}$	$\frac{mN}{t^2}$
DK-STP-CS	$y = \Phi_3 \rtimes x$	$\Phi_3 \in \mathbb{R}^{m \times \frac{N}{\gamma}}$	$\frac{mN}{\gamma}$	$\frac{mN}{\gamma}$

In Figure 9, the x-axis represents the compression ratio ranging from 0.05 to 0.5 with intervals of 0.05, while the y-axis represents the PSNR values of the images before and after reconstruction. From the curves in the figures, it can be observed that the PSNR values for all three curves gradually increase as the compression ratio rises. The Gaussian and Bernoulli curves exhibit a smooth trend, with the PSNR values increasing uniformly as the compression ratio rises. Moreover, the experimental data for these two curves are closely aligned, and their overall trajectories are nearly identical, demonstrating stability across various sampling scenarios. In contrast, the recovery performance of the Toeplitz curve is generally inferior to the other two curves, particularly at lower sampling rates, where its effectiveness is notably weaker. As x increases, the curve exhibits rapid growth when x is less than 0.1, followed by a fluctuating increase between $x = 0.1$ and $x = 0.4$. When x exceeds 0.4, the growth rate accelerates significantly. As x approaches 0.5, the PSNR values improve substantially, nearly matching or even surpassing the recovery performance of the other two curves.

Through the comparative experiments conducted above, we find that DK-STP-CS demonstrates significant advantages in terms of anti-interference capability and image reconstruction quality. From the perspective of memory efficiency, it also outperforms traditional CS methods. However, the experiments reveal that introducing inter-group correlation can affect the success rate of reconstruction to some extent, which further emphasizes the importance of selecting an appropriate measurement matrix. Choosing a structurally stable measurement matrix is essential. From a computational time perspective, DK-STP-CS achieves the predefined error threshold more easily through iterations. For tasks related to image storage and recovery, DK-STP-CS offers notable improvements. Using PSNR as the metric to evaluate the quality of reconstructed images, the enhanced DK-STP-CS exhibits clear advantages.

4.5 Complexity analysis and discussion on deep learning methods

Analyzing model complexity is crucial for evaluating algorithmic efficiency. While Ref. [28] establishes the complexity relationships between CS and STP-CS, we further provide in Table 3 a comprehensive comparison of both computational and storage complexity among DK-STP-CS and these two baseline methods. The storage matrix here refers to the matrix that needs to be preserved in practical computations. The storage space represents the number of elements in the stored matrix, while the sampling complexity corresponds to the number of matrix-vector multiplications required during computation.

To comprehensively evaluate the three methods across multiple dimensions, we employ a broader set of metrics to characterize the experimental results. Specifically, PSNR, SSIM, and running time are utilized to compare performance under varying sampling rates, as shown in Figure 10. In order to minimize the potential bias introduced by individual image characteristics, the evaluation is conducted on randomly sampled image patches from the Set5 dataset, thereby demonstrating the generalizability of the methods. It is noteworthy that at a compression ratio of 0.5, the DK-STP-CS method demonstrates a significant reduction in computational time, while under other conditions the runtime remains comparable to other methods. This observation provides valuable guidance for selecting appropriate γ values in practical applications to optimize computational efficiency without compromising reconstruction quality.

With the rapid advancement of deep learning, numerous data-driven approaches have been introduced to CS. In CS, the design of measurement matrices and reconstruction algorithms remains a critical challenge. Deep learning methods address this by learning optimized measurement matrices directly from training datasets, offering a principled and adaptive alternative to traditional matrix constructions. Furthermore, while conventional CS reconstruction relies on iterative optimization to approximate solutions, deep learning models employ multi-layer neural networks to directly predict reconstructed signals. This paradigm shift not only substantially improves reconstruction quality but also significantly enhances computational efficiency. In Table 4, we present a comparative analysis of PSNR values between DK-STP-CS and three deep learning-based methods under varying sampling rates. It can be clearly observed that the deep learning approaches achieve significantly superior reconstruction performance compared to traditional iterative methods.

• Reconstruction accuracy: In terms of reconstruction accuracy, the two categories of algorithms exhibit distinct characteristics. Traditional algorithms, grounded in rigorous sparse assumptions and mathematical theory, demonstrate stable performance within theoretically guaranteed bounds. However, under extremely low sampling rates,

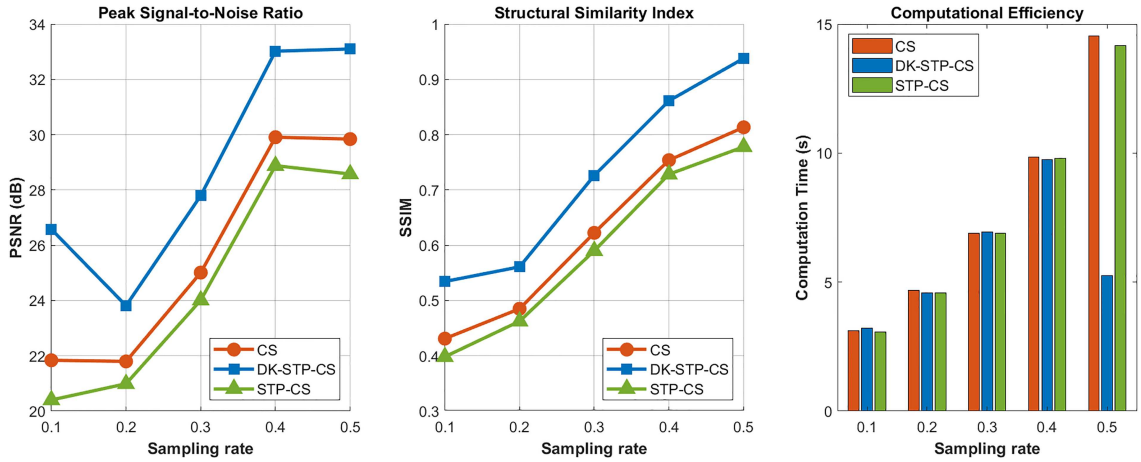

Figure 10 (Color online) Comparative results of PSNR, SSIM, and running time on five images (64×64) from the Set5 dataset, using a Gaussian random measurement matrix and BP as the reconstruction method.

Table 4 Performance comparison (dB) of different algorithms at various sampling ratios on Set11 [21]. The ReconNet, ISTA-Net and CSNet* data are from the previous study [23].

Algorithm	Sampling ratio					
	0.5	0.4	0.3	0.1	0.01	Average
DK-STP-CS	31.16	30.21	28.51	22.51	11.29	25.28
ReconNet	31.50	30.58	28.74	24.28	17.27	26.47
ISTA-Net	37.43	35.36	32.91	25.80	17.30	29.76
CSNet*	37.51	36.10	33.86	28.10	20.94	31.30

their reliance on handcrafted priors reveals limitations, often resulting in blurred reconstructions and noticeable artifacts, accompanied by rapid degradation in accuracy. In contrast, deep learning methods adopt a data-driven approach, enabling them to learn substantially more complex signal priors from training datasets than conventional sparse transformations. Consequently, they generally achieve significantly higher quantitative metrics and superior visual quality in most scenarios. But the accuracy advantage of deep learning is highly dependent on the consistency between test and training data distributions, and their generalization capability and robustness typically fall short of traditional methods, particularly under data distribution shifts or unseen scenarios.

• Computational efficiency: When comparing computational efficiency, the two approaches demonstrate complementary strengths at different stages. Traditional algorithms concentrate their computational cost in the iterative reconstruction process, which becomes particularly time-consuming for high-dimensional signals and often fails to meet the demands of real-time applications. In contrast, deep learning methods shift the substantial computational burden to the training phase. While this process requires extensive datasets and substantial GPU resources over prolonged periods, it enables extremely efficient online reconstruction once training is complete. The inference stage merely requires a single forward propagation through the network, achieving reconstruction speeds that are orders of magnitude faster than traditional iterative methods. It is observed that reconstructing an image using a pre-trained model typically requires less than one second in [23]. In contrast, our algorithm demands several hours of computation time for larger images under identical CPU and GPU. This characteristic grants deep learning approaches a significant advantage in inference efficiency, making them particularly suitable for real-time processing scenarios.

• Model complexity: In terms of model complexity, the two approaches differ fundamentally. Traditional algorithms exhibit extremely low model complexity, with their core components consisting of predefined measurement matrices and sparse transformation bases. These algorithms follow fixed procedures with minimal parameters, resulting in systems characterized by high interpretability and solid theoretical guarantees. In contrast, deep learning algorithms demonstrate exceptionally high model complexity, typically incorporating millions or even more learnable parameters that form powerful "black-box" models. While this complexity enables remarkable representational learning capacity, it simultaneously introduces challenges including difficulties in theoretical analysis, unpredictable generalization performance, and heavy reliance on training data. These limitations pose significant challenges for deployment in domains requiring high levels of security and trustworthiness.

Deep learning methods require substantial amounts of data for effective training. When faced with data distri-

butions different from the training set, their generalization capability tends to be considerably limited. In contrast, traditional iterative methods demonstrate consistent performance across various types of information, exhibiting stronger generalization capacity. Therefore, selecting the appropriate model according to specific circumstances, or even combining the strengths of both approaches, becomes crucial for maximizing overall performance.

5 Conclusion and future work

In this work, a novel CS approach named DK-STP-CS was developed, where the measurement matrix was enhanced through the application of a special semi-tensor product (DK-STP). The technical contributions encompass three key aspects: (1) formal derivation of mathematical properties and operational algorithms for the DK-STP-CS framework, (2) innovative integration of intra-group correlation analysis to optimize measurement matrices through multi-dimensional feature interaction, and (3) systematic validation through image reconstruction experiments demonstrating consistent performance improvements over conventional CS and STP-CS approaches. Empirical results confirmed that the proposed method achieves superior reconstruction fidelity with enhanced noise robustness while maintaining memory efficiency. The framework exhibits accelerated convergence to target error thresholds compared to baseline methods. A comparative analysis of measurement matrices provides operational guidelines for practical implementations. Future work will focus on memory optimization through sparse tensor architectures, hybrid model-learning frameworks, and advanced group correlation analysis using machine learning techniques for adaptive measurement matrix generation.

Acknowledgements This work was supported by National Natural Science Foundation of China (Grant Nos. 62273201, 62350037) and Taishan Scholar Project of Shandong Province of China (Grant No. TSTP20221103).

References

1 Donoho D L. Compressed sensing. IEEE Trans Inform Theor, 2006, 52: 1289–1306
2 Baraniuk R. Compressive sensing. IEEE Signal Process Mag, 2007, 24: 118–121
3 Nyquist H. Certain topics in telegraph transmission theory. Proc IEEE, 2002, 90: 280–305
4 Mallat S G, Zhang Z F. Matching pursuits with time-frequency dictionaries. IEEE Trans Signal Process, 1993, 41: 3397–3415
5 Candès E J, Tao T. Decoding by linear programming. IEEE Trans Inf Theory, 2005, 51: 4203–4215
6 Foucart S. A note on guaranteed sparse recovery via ℓ_1-minimization. Appl Comput Harmonic Anal, 2010, 29: 97–103
7 Bruckstein A M, Donoho D L, Elad M. From sparse solutions of systems of equations to sparse modeling of signals and images. SIAM Rev, 2009, 51: 34–81
8 Candès E J. The restricted isometry property and its implications for compressed sensing. CR Math, 2008, 346: 589–592
9 Laska J N, Boufounos P T, Davenport M A, et al. Democracy in action: quantization, saturation, and compressive sensing. Appl Comput Harmonic Anal, 2011, 31: 429–443
10 Lustig M, Donoho D, Pauly J M. Sparse MRI: the application of compressed sensing for rapid MR imaging. Magn Reson Med, 2007, 58: 1182–1195
11 Bu H X, Bai X, Tao R. Compressed sensing SAR imaging based on sparse representation in fractional Fourier domain. Sci China Inf Sci, 2012, 55: 1789–1800
12 Arce G R, Brady D J, Carin L, et al. Compressive coded aperture spectral imaging: an introduction. IEEE Signal Process Mag, 2014, 31: 105–115
13 Li L C, Li D J, Pan Z H. Compressed sensing application in interferometric synthetic aperture radar. Sci China Inf Sci, 2017, 60: 102305
14 Haupt J, Bajwa W U, Rabbat M, et al. Compressed sensing for networked data. IEEE Signal Process Mag, 2008, 25: 92–101
15 Bajwa W U, Haupt J D, Raz G M, et al. Toeplitz-structured compressed sensing matrices. In: Proceedings of the 14th IEEE/SP Workshop Stat Signal Process, 2007. 294–298
16 Yu L, Barbot J P, Zheng G, et al. Compressive sensing with chaotic sequence. IEEE Signal Process Lett, 2010, 17: 731–734
17 Cheng D, Qi H, Xue A. A survey on semi-tensor product of matrices. Jrl Syst Sci Complex, 2007, 20: 304–322
18 Xie D, Peng H, Li L, et al. Semi-tensor compressed sensing. Digital Signal Processing, 2016, 58: 85–92
19 Hu Y, Huang S, Zhao L, et al. Narrowband interference cancellation for OFDM based on deep learning and compressed sensing. IEEE Trans Signal Process, 2025, 73: 1612–1625
20 Li L, Fang Y, Liu L, et al. Overview of compressed sensing: sensing model, reconstruction algorithm, and its applications. Appl Sci, 2020, 10: 5909
21 Kulkarni K, Lohit S, Turaga P, et al. ReconNet: non-iterative reconstruction of images from compressively sensed measurements. In: Proceedings of the IEEE/CVF Conference on Computer Vision and Pattern Recognition, 2016. 449–458
22 Zhang J, Ghanem B. ISTA-Net: interpretable optimization-inspired deep network for image compressive sensing. In: Proceedings of the IEEE/CVF Conference on Computer Vision and Pattern Recognition, 2018. 1828–1837
23 Shi W, Jiang F, Liu S, et al. Image compressed sensing using convolutional neural network. IEEE Trans Image Process, 2020, 29: 375–388
24 Qi Q, Feng J E. From DK-STP to a set of Lie bracket. MMC, 2025, 5: 410–420
25 Cheng D. From DK-STP to non-square general linear algebra and general linear group. Commun Inf Syst, 2024, 24: 1–60
26 Welch L. Lower bounds on the maximum cross correlation of signals (Corresp.). IEEE Trans Inform Theor, 1974, 20: 397–399
27 Strohmer T, Heath J R W. Grassmannian frames with applications to coding and communication. Appl Comput Harmonic Anal, 2003, 14: 257–275
28 Liang J, Peng H, Li L, et al. Construction of structured random measurement matrices in semi-tensor product compressed sensing based on combinatorial designs. Sensors, 2022, 22: 8260